PHYSICAL REVIEW A VOLUME 38, NUMBER 5 SEPTEMBER 1, 1988

Coupled-channel theory of excitation and charge transfer in relativistic atomic collisions

Nobuyuki Toshima* and Jörg Eichler†
Bereich Kern- und Strahlenphysik, Hahn-Meitner-Institute Berlin, D-1000 Berlin 39, Federal Republic of Germany
(Received 21 March 1988)

The theory for a fully relativistic, two-center, coupled-channel treatment of atomic collisions between high-Z ions has been developed and applied to $U^{92+}+U^{91+}$ collisions at 500 MeV/amu and to $Xe^{54+}+Ag$ and $Xe^{54+}+Au$ collisions at 82, 140, and 197 MeV/amu. In the former case, a set of 36, and in the latter a set of up to 29 atomic Dirac basis states has been used. Detailed state-to-state cross sections for excitation and charge transfer are presented. For charge transfer in $Xe^{54+}+Ag$ and $Xe^{54+}+Au$ collisions, the calculated results are generally in good agreement with experimental data. Relativistically induced magnetic couplings of unusually long range are identified and classified with respect to their selection rules and range dependences.

I. INTRODUCTION

In recent years, the study of atomic collisions at relativistic projectile velocities has developed into a new field of physics. At the Berkeley Bevalac, ion beams ranging from carbon to uranium projectiles are now produced with maximum energies of about 1 GeV/amu. It is then possible to examine quantum electrodynamics (QED) by measuring the Lamb shift at very high charge numbers Z. For this purpose, uranium ions have been accelerated up to 1 GeV/amu, and in subsequent beam-foil time-of-flight measurements the produced hydrogenlike or heliumlike uranium ions have been studied.[1] Furthermore, the atomic structure of high-Z few-electron ions, as well as dynamic processes, may be investigated. For the design and interpretation of such experiments, it is necessary to calculate excitation and charge transfer cross sections for relativistic projectile velocities and relativistic electron motions.[2,3]

Excitation and ionization cross sections in relativistic collisions have been calculated by Anholt *et al.*[4] and by Becker *et al.*[5] in a first-order perturbation theory. Electron capture has been successfully treated by Eichler,[6,7] Anholt and Eichler,[8] and by Meyerhof *et al.*[9] with a relativistic eikonal approximation. Earlier calculations using a relativistic Oppenheimer-Brinkman-Kramers (OBK) approximation[10] resulted in cross sections that were almost an order of magnitude too large. Other perturbative approaches have also been employed; for example, higher-order OBK expansions,[11] the impulse approximation,[12] continuum distorted-wave methods,[13] the symmetrized eikonal approximation,[14] and a relativistic first-order Born approximation with Coulomb boundary conditions[15] (R1B).

Recently, Becker *et al.*[16] used a finite-difference algorithm as a nonperturbative method to calculate inner-shell excitation and ionization for $U^{92+}+U^{91}$ collisions at 1 GeV/amu. Their exploratory computations were, however, confined to the impact parameter $b=0$ (which carries zero weight for the cross section). To supplement those results, Becker has also performed coupled-channel calculations using a one-center expansion in terms of target bound and discretized continuum states.[17] In this method, the projectile merely acts as a moving source for an electromagnetic field. Molecular effects during the collision and the possibility of charge transfer are hence disregarded.

In the current work we solve the time-dependent Dirac equation for relativistic ion-atom collisions employing a coupled-channel treatment with a two-center atomic expansion for arbitrary impact parameters. A brief account has been given in Ref. 18. Within this method, the only approximation consists in the restriction to a finite set of (up to 36) atomic basis states (as compared to 20 in Ref. 18). In most cases, we couple $1s_{1/2}$, $2s_{1/2}$, $2p_{1/2}$, $2p_{3/2}$, $3s_{1/2}$, $3p_{1/2}$, and $3p_{3/2}$ states of target and projectile.

Just as in nonrelativistic collisions,[19] the two-center atomic expansion is most appropriate if the projectile speed is of the same order as the orbital velocity of the active electron and hence molecular effects play a role (for details see Sec. IV). In other words, with the coupled-channel treatment we aim at "slow" relativistic collisions with laboratory projectile energies ranging between about 100 MeV/amu and 1 GeV/amu, depending on the nuclear charges involved. Incidentally, this is the energy regime in which most experiments have been done.

Since in the current work the expansion is restricted to a finite set of bound atomic eigenstates, we are able to describe excitation and transfer within this set to arbitrary order, but so far we have not included ionization channels. The approximate treatment of higher excited levels and of continuum states is left to a future publication. Experience from nonrelativistic calculations suggests (see Sec. IV) that the rates for charge exchange will not be altered significantly by including these channels.

The aim of our paper is threefold. Firstly, we want to develop, in some detail, the formalism for fully relativistic two-center close-coupling calculations. As one may expect, the main complications compared to the familiar nonrelativistic problem[19] arise from the basis functions attached to the relativistically moving projectile. Secondly, we wish to demonstrate the feasibility of detailed calculations for the $U^{92+}+U^{91+}$ system which serves as a

testing ground for fully relativistic collisions (in which the relativistic electron motion plays a significant role) in a similar way as does the $p+H$ system for nonrelativistic encounters. Thirdly, in two cases, namely, $Xe^{54+}+Ag$ and $Xe^{54+}+Au$ we want to compare calculated results with experimental cross-section data.[9,20] Additional experimental data for projectile K capture into Xe^{54+} can be extracted from Xe^{54+} and Xe^{52+} data. Unfortunately, only *total* cross sections are experimentally available, so that a test cannot be very specific.

The plan of the paper is as follows. In Sec. II we give an outline of the theory and subsequently, in Sec. III, some numerical details. The results of our calculations are presented and discussed in Sec. IV, while Sec. V contains some concluding remarks. Atomic units (a.u.) are used throughout unless specifically stated otherwise.

II. THEORY

Let us consider a relativistic projectile ion (charge Z_P) colliding with a one-electron target atom with nuclear charge Z_T. At relativistic velocities v, it is a very good approximation for atomic processes to assume a classical rectilinear trajectory $\mathbf{R}=\mathbf{b}+\mathbf{v}t$ for the projectile motion. Here, $\mathbf{R}$ is the projectile position with respect to the target nucleus, and $\mathbf{b}$ is the impact parameter . Associated with the two inertial frames, we have two sets of space-time coordinates. While $\mathbf{R}$ and $\mathbf{r}_T,t$ measure the positions of projectile nucleus and electron, respectively, from the target nucleus, the coordinates $\mathbf{R}'$ and $\mathbf{r}'_P,t'$ refer to the positions of the target nucleus and electron, respectively, as seen from the projectile nucleus. Both sets of space-time coordinates are connected by a Lorentz transformation characterized by the parameters $\beta=v/c$, $\gamma=(1-\beta^2)^{-1/2}$, $\delta=[(\gamma-1)/(\gamma+1)]^{1/2}$, where $c\simeq 137$ a.u. is the speed of light.

The time-dependent two-center Dirac equation governing the electron motion in the laboratory (target) system is given by

$$\left[H-i\frac{\partial}{\partial t}\right]\Psi(\mathbf{r}_T,t)=0\ , \tag{1}$$

with

$$H=-ic\boldsymbol{\alpha}\cdot\boldsymbol{\nabla}-\frac{Z_T}{r_T}-S^2\frac{Z_P}{r'_P}+c^2\gamma_4\ , \tag{2}$$

where α_x, α_y, α_z (the z axis being chosen in the beam direction), and γ_4 are the familiar Dirac matrices, and the spinor transformation[21]

$$S=\left[\frac{\gamma+1}{2}\right]^{1/2}(1-\delta\alpha_z)=S^{\dagger} \tag{3a}$$

with

$$S^2=\gamma(1-\beta\alpha_z) \tag{3b}$$

transforms a four-spinor from the target to the projectile system according to

$$\psi'(\mathbf{r}',t')=S\psi(\mathbf{r},t)\ . \tag{4}$$

The Hamiltonian (2) does not include[15] the interaction[22] Z_PZ_T/R' with $R'=(b^2+\gamma^2v^2t^2)^{1/2}$ between the two nuclear point charges, since it does not contribute to the total cross-section or b-dependent transition probability. Starting from expression (2), it is convenient to introduce the target Hamiltonian and the target eigenfunctions in the target system through

$$H_T=-ic\boldsymbol{\alpha}\cdot\boldsymbol{\nabla}-\frac{Z_T}{r_T}+c^2\gamma_4 \tag{5a}$$

and

$$\left[H_T-i\frac{\partial}{\partial t}\right]\psi_k(\mathbf{r}_T,t)=0\ ,\qquad \psi_k(\mathbf{r}_T,t)=\phi_k(\mathbf{r}_T)e^{-iE_kt}\ . \tag{5b}$$

Similarly, the projectile Hamiltonian and the associated eigenfunctions in the projectile system are

$$H'_P=-ic\boldsymbol{\alpha}\cdot\boldsymbol{\nabla}'_P-\frac{Z_P}{r'_P}+c^2\gamma_4 \tag{6a}$$

and

$$\left[H'_P-i\frac{\partial}{\partial t'}\right]\psi_{k'}(\mathbf{r}'_P,t')=0\ ,\qquad \psi_{k'}(\mathbf{r}'_P,t')=\phi_{k'}(\mathbf{r}'_P)e^{-iE_{k'}t'}\ . \tag{6b}$$

In our coupled-channel treatment we use a two-center atomic expansion of the total wave function Ψ in terms of target and projectile atomic orbitals (AO). In this way, molecular wave functions in the interaction zone (for not-too-small impact parameters) can approximately be represented,[19] and it is a simple matter to specify the initial conditions at $t\rightarrow-\infty$. It is well known from nonrelativistic calculations[19] that for collision velocities neither much smaller nor much larger than the relevant orbital velocity v_e of the electron, mainly distant collisions are important and hence two-center AO expansions are capable of describing the time-dependent wave function in the interaction region. Referring the total wave function to the laboratory system we therefore start from the expansion

$$\Psi(\mathbf{r},t)=\sum_k a_k(t)\psi_k(\mathbf{r}_T,t)+\sum_{k'}a_{k'}(t)S^{-1}\psi_{k'}(\mathbf{r}'_P,t')\ . \tag{7}$$

The first sum represents an expansion in terms of target states; the second sum is an expansion in terms of projectile states originally defined in the projectile rest system and subsequently transformed to the laboratory system. In practice, both expansions are truncated to a finite set so that the problem of overcompleteness does not arise. Note that the Lorentz transformation of the time factor included in the projectile states automatically implies[6] the relativistic counterparts of the well-known translation factors. Moreover, there is no need to expand in terms of distorted waves, explicitly satisfying relativistic Coulomb boundary conditions[15] since their effect can be absorbed

into a b-dependent phase of the expansion coefficients.[23]

When inserting Eq. (7) into Eq. (1) we immediately verify that

$$\left[H-i\frac{\partial}{\partial t}\right]\psi_k=\left[H_T-i\frac{\partial}{\partial t}-S^2\frac{Z_P}{r'_P}\right]\psi_k$$
$$=-S^2\frac{Z_P}{r'_P}\psi_k\ , \tag{8a}$$

and, using the transformation properties of the Dirac equation, we get

$$\left[H-i\frac{\partial}{\partial t}\right]S^{-1}\psi_{k'}=\left[S\left[H'_P-i\frac{\partial}{\partial t'}\right]S-\frac{Z_T}{r_T}\right]S^{-1}\psi_{k'}$$
$$=-\frac{Z_T}{r_T}S^{-1}\psi_{k'}\ . \tag{8b}$$

With the aid of Eqs. (8), the time-dependent two-center Dirac equation (1) can be rewritten as a set of coupled differential equations for the occupation amplitudes $a_k(t)$ and $a_{k'}(t)$. Combining the amplitudes into a column vector $\underline{a}=(a_k,\ldots;a_{k'},\ldots)^T$ we may write the coupled equations in a compact matrix form as

$$i\underline{N}\,\dot{\underline{a}}=\underline{V}\,\underline{a} \tag{9}$$

or

$$\dot{\underline{a}}=-i\underline{N}^{-1}\underline{V}\,\underline{a}\ . \tag{10}$$

The overlap matrix $\underline{N}$ and the interaction matrix $\underline{V}$ are each built from four submatrices corresponding to target-target, target-projectile, projectile-target, and projectile-projectile transitions.

The overlap matrices are

$$N_{ik}=\delta_{ik}e^{-i(E_k-E_i)t}\ , \tag{11a}$$

$$N_{ik'}=\int\phi_i^\dagger(\mathbf{r}_T)S^{-1}\phi_{k'}(\mathbf{r}'_P)e^{i\gamma E_{k'}(v/c^2)z_T}d^3r_T\times e^{-i(\gamma E_{k'}-E_i)t}\ , \tag{11b}$$

$$N_{i'k}=\int\phi_{i'}^\dagger(\mathbf{r}'_P)S^{-1}\phi_k(\mathbf{r}'_P)e^{-i\gamma E_{i'}(v/c^2)z_T}d^3r_T\times e^{-i(E_k-\gamma E_{i'})t}\ , \tag{11c}$$

$$N_{i'k'}=\delta_{i'k'}e^{-i\gamma(E_{k'}-E_{i'})t}\ . \tag{11d}$$

The last equation (11d) expressing the orthogonality of the projectile eigenstates in the target system can be directly proved by using the transformation properties of the Dirac equation (1). Similarly, we have four types of interaction matrix elements

$$V_{ik}=\int\phi_i^\dagger(\mathbf{r}_T)\left[-S^2\frac{Z_P}{r'_P}\right]\phi_k(\mathbf{r}_T)d^3r_Te^{-i(E_k-E_i)t}\ , \tag{12a}$$

$$V_{ik'}=\int\phi_i^\dagger(\mathbf{r}_T)\left[-S^{-1}\frac{Z_T}{r_T}\right]\phi_{k'}(\mathbf{r}'_P)e^{i\gamma E_{k'}(v/c^2)z_T}d^3r_T\times e^{-i(\gamma E_{k'}-E_i)t}\ , \tag{12b}$$

$$V_{i'k}=\int\phi_{i'}^\dagger(\mathbf{r}'_P)\left[-S\frac{Z_P}{r'_P}\right]\phi_k(\mathbf{r}_T)e^{-i\gamma E_{i'}(v/c^2)z_T}d^3r_T\times e^{-i(E_k-\gamma E_{i'})t}\ , \tag{12c}$$

$$V_{i'k'}=\int\phi_{i'}^\dagger(\mathbf{r}'_P)\left[-S^{-2}\frac{Z_T}{r_T}\right]\phi_{k'}(\mathbf{r}'_P)\times e^{-i\gamma(E_{k'}-E_{i'})(v/c^2)z_T}d^3r_T\times e^{-i\gamma(E_{k'}-E_{i'})t}\ . \tag{12d}$$

One may easily verify that in the nonrelativistic limit all matrix elements merge into the corresponding nonrelativistic expressions including translation factors.

In principle, the set of coupled equations (10) is equivalent to the original two-center Dirac equation (1). In practice, however, the expansion (7) has to be truncated to a finite number of eigenstates. The choice of this truncated set hence constitutes the only approximation in solving the problem.

Before Eqs. (10) can be solved numerically, we specify the target electron initially to be in state k_0 so that

$$a_{k_0}(t=-\infty)=1\ ,$$
$$a_k(t=-\infty)=0\ \text{ for } k\neq k_0\ , \tag{13}$$
$$a_{k'}(t=-\infty)=0$$

constitute the initial conditions.

It is noted that, in our expansion in terms of atomic eigenfunctions, all basis states are mutually orthogonal at asymptotic separations, i.e., for $t\to\pm\infty$. This means that the expansion coefficients $a_k,a_{k'}$ can be interpreted unambiguously as occupation amplitudes (in this limit) and, in particular, there is no overlap with the negative-energy continuum which might lead to spurious results. In the interaction region, where target and projectile states are nonorthogonal and where each bound state of one center has some overlap with bound states and positive- as well as negative-energy continuum states of the other center, an interpretation in terms of occupation amplitudes is not needed. It suffices that the overlap matrix (11) is rigorously taken into account.

The final occupation probabilities are

$$P_k(b)=|\,a_k(t=\infty)\,|^2\ \text{ for excitation} \tag{14a}$$

and

$$P_{k'}(b)=|\,a_{k'}(t=\infty)\,|^2\ \text{ for charge transfer}\ . \tag{14b}$$

The integrated partial cross section for exciting state k from the initial state k_0 is given by

$$\sigma_k=2\pi\int_0^\infty P_k(b)b\,db\ , \tag{15}$$

while for charge transfer, k has to be replaced by k'.

The main task consists in evaluating the matrix elements defined by Eqs. (11) and (12). In doing so we use exact hydrogenic Dirac wave functions[24] as basis states ϕ_k and $\phi_{k'}$ and the associated eigenenergies. It is immediately seen that owing to the Lorentz transformation of the space-time coordinate there is no axial symmetry about the internuclear line which in a nonrelativistic collision greatly facilitates the evaluation of the two-center matrix elements. A fully numerical integration is hence required. In the following section we briefly discuss the numerical procedure.

III. NUMERICAL PROCEDURE

The most cumbersome part in solving Eq. (10) consists in the evaluation of the matrix elements (11) and (12). For a given projectile energy, these matrix elements have to be computed at each time t and each impact parameter b.

It is helpful first to notice that calculations can be confined to times $t \geq 0$, i.e., after the closest approach of the projectile to the target nucleus has been reached. The incoming branch of the trajectory ($t \leq 0$) can be mapped upon the outgoing branch ($t \geq 0$) by rotating the coordinate system about the internuclear line at $t=0$ (chosen as x axis) by an angle of π. With the resulting replacements $t \rightarrow -t$, $x \rightarrow x$, $y \rightarrow -y$, and $z \rightarrow -z$, we can exploit the relation

$$Y_l^m(\pi-\theta, 2\pi-\phi)=(-1)^{l+m}(Y_l^m)^*(\theta,\phi)$$

for the spherical harmonics to derive the symmetry relations

$$N_{\alpha\beta}(t)=(-1)^{l_A^\alpha+l_A^\beta+m_j^\alpha+m_j^\beta+1}N^*_{\alpha\beta}(-t) \tag{16a}$$

and

$$V_{\alpha\beta}(t)=(-1)^{l_A^\alpha+l_A^\beta+m_j^\alpha+m_j^\beta+1}V^*_{\alpha\beta}(-t)\ , \tag{16b}$$

where α,β denote any of the labels i,k,i',k' and $l_A^{\alpha,\beta}$ are the orbital angular momenta for the large components of the states α,β, while $m_j^{\alpha,\beta}$ are the projections of the total angular momentum $j=l_A\pm\frac{1}{2}$. Both relations may be combined to yield

$$(\underline{N}^{-1}\underline{V})_{\alpha\beta}(t)=(-1)^{l_A^\alpha+l_A^\beta+m_j^\alpha+m_j^\beta+1}(\underline{N}^{-1}\underline{V})^*_{\alpha\beta}(-t)\ , \tag{17}$$

which is directly applicable in Eq. (10).

The computation of all matrix elements is performed by direct three-dimensional numerical integration in coordinate space.

The single-center matrix elements V_{ik} and $V_{i'k'}$ are calculated in spherical coordinates (r_T,θ_T,ϕ_T) and (r_P,θ_P,ϕ_P) for target and projectile states, respectively. Only at small internuclear distances R, where the convergence of the integrals becomes unsatisfactory, are integrations performed in prolate spheroidal coordinates.

Similarly, the two-center matrix elements $N_{ik'},N_{i'k}$, $V_{ik'}$, $V_{i'k}$ are evaluated in prolate spheroidal coordinates

$$\xi=(r_1+r_2)/R,\quad \eta=(r_1-r_2)/R$$

and ϕ, where r_1 and $r_2=|\mathbf{R}-\mathbf{r}_1|$ are the electron-target and electron-projectile separations in the coordinate system rotating with the internuclear line in the laboratory frame. Since for each point (ξ,η,ϕ) in this system, the atomic wave functions have to be furnished, we pass through the following sequence of transformations: $(\xi,\eta,\phi)\rightarrow(r_1,r_2,\phi)\rightarrow(x_r,y_r,z_r)$ in the rotating coordinate system. From here, the Cartesian coordinates (x_T,y_T,z_T) in the space-fixed laboratory system can be obtained and are used to evaluate the target wave function and r_T. Finally, a simple Lorentz boost assigns a set (x'_P,y'_P,z'_P,t') to each set (x_T,y_T,z_T,t) thus allowing us to evaluate the projectile wave function and r'_P.

The Gauss-Laguerre and Gauss-Legendre procedures are subsequently used to perform the quadratures for $dr,d\xi$ and for $d\theta$, $d\phi$, and $d\eta$, respectively. The number of mesh points varies between 10 and 200 depending on the value of R.

Owing to Eq. (17) it is sufficient to calculate the matrix elements at discrete time steps for $t \geq 0$ and to interpolate between the mesh points. It is economical to divide the range of t into an inner and an outer region. Estimating the characteristic radius of the interaction region by $\bar{r}=4/(Z_P+Z_T)$ we define the inner region by $|vt| \leq 20\bar{r}$ and the outer region by $20\bar{r}<|vt|250\bar{r}$. When necessary for convergence, the upper limit has been extended to $500\bar{r}$ or $1000\bar{r}$. Within the inner region, we calculate and tabulate all matrix elements at 40 mesh points. An interpolated value then deviates from an exact one by less than 0.1%. In the outer region, the two-center matrix elements are negligibly small and it suffices to calculate and store the single-center matrix elements at 60 mesh points.

The coupled equations (10) with the initial condition (13), are then solved by Milne's predictor-corrector method. In this algorithm, the step width in time is automatically adjusted for any desired accuracy. For the b integration entering into the evaluation of the cross section (15) we used up to 40 mesh points.

We have performed several checks of our numerical calculations. We have examined the convergence of the matrix elements and also compared with cases in which a partially analytical evaluation is possible.[6] We have made sure that for small velocities and small charges our results merge into those of independently calculated nonrelativistic cross sections. Furthermore, for each calculation, we verify that the unitarity requirement is satisfied to an accuracy of better than 10^{-4}. Finally, as a very stringent test, we find that for all cases examined, detailed balancing for target excitation as well as for charge transfer is valid within an accuracy of 10^{-2} to 10^{-3}. It should be mentioned that the calculations require considerable computing time.

IV. RESULTS AND DISCUSSION

As is well known from nonrelativistic collisions,[19] the coupled-channel formalism with two-center atomic expansions is best applied if the projectile velocity is of the

same order as the orbital velocity of the active electron. For relativistic collisions, the matching energy E_m is estimated by the requirement[6] that the kinetic energy of a free electron traveling with the speed of the projectile equals the binding energy of the atomic state, or $\gamma-1=1-(1-\alpha^2Z^2)^{1/2}$ for $1s$ states. There are other possible prescriptions yielding similar results.

In this sense, we are dealing here with "slow" relativistic collisions. In the following, we consider the collision systems of $U^{92+}+U^{91+}$ at 500 MeV/amu ($E_m^U=240$ MeV/amu) and of $Xe^{54+}+Ag$ and $Xe^{54+}+Au$ at 82, 140, and 197 MeV/amu ($E_m^{Ag}=55$ MeV/amu, $E_m^{Au}=170$ MeV/amu). The U + U collision mainly serves as a model case for which effects of relativistic electron and projectile motion can be studied, but experimental data are not yet available. For $Xe^{54+}+Ag$ and $Xe^{54+}+Au$ we may compare with experimental data for single-electron transfer.

A. Collision of $U^{92+}+U^{91+}$

This collision serves as a testing ground for various theoretical approaches.[15–17] In a previous paper,[18] we discussed a 20-state coupled-channel calculation involving target and projectile $1s_{1/2}$, $2s_{1/2}$, $2p_{1/2}$, and $2p_{3/2}$ shells. In the present calculation at a projectile energy of 500 MeV/amu, we have supplemented the basis of Ref. 18 by $3s_{1/2}$, $3p_{1/2}$, and $3p_{3/2}$ states at target and projectile so that altogether 36 exact hydrogenic bound states are coupled.

In Figs. 1 and 2 we present the time evolution of the occupation probabilities for target shells (excitation) and

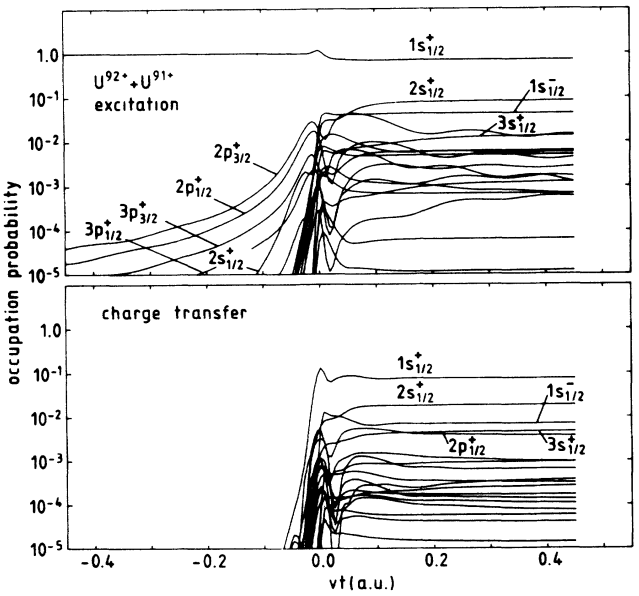

FIG. 1. Time evolution of the occupation probabilities of target and projectile states in $U^{92+}+U^{91+}(1s_{1/2})$ collisions at 500 MeV/amu laboratory energy and impact parameter $b=0.01$ a.u. The abscissa plotted is the projection of the projectile-target separation on the beam direction. The projection of the angular momentum is indicated by +, −, and + + for $m_j=\frac{1}{2}$, $-\frac{1}{2}$, and $\frac{3}{2}$, respectively.

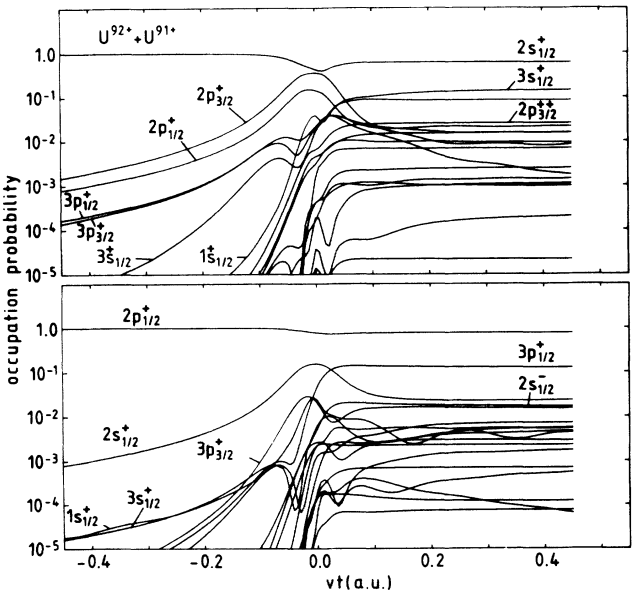

FIG. 2. Time evolution of the occupation probabilities of the target states in $U^{92+}+U^{91+}(2s_{1/2})$, $U^{91+}(2p_{1/2})$ collisions at 500 MeV/amu laboratory energy and impact parameter $b=0.01$ a.u. For the notation see caption of Fig. 1.

projectile shells (charge transfer) assuming an impact parameter of 0.01 a.u. This is approximately equal to the K-shell radius and roughly corresponds to the region of maximum contribution to the cross section, see Fig. 3. Regarding the interval $|vt|\leq 40a_K$ displayed in Figs. 1 and 2, it should be mentioned that it just represents a narrow window out of the total time range $|vt|\leq(500-2000)a_K$ actually treated in the calculations, see Sec. III. As has been noted in Sec. II, the interpretation of the expansion coefficients as probability amplitudes is valid only approximately near $t=0$, so that transient probabilities exceeding 1 may occur. While Fig. 1 shows excitation and charge transfer from an initial $1s_{1/2}$ ground state, Fig. 2 refers to target excitation (or deexcitation) from initially excited $2s_{1/2}$ and $2p_{1/2}$ states.

Both figures reveal three qualitative features: (a) nonperturbative multistep processes are important; (b) electron transfer, both during the collision as well as in the exit channel, is of equal magnitude as excitation and hence cannot be neglected;[17] (c) certain target states are affected by the projectile long before and long after it reaches its distance of closest approach at $t=0$. These anomalous long-range couplings are of a relativistic origin and are entirely absent in nonrelativistic coupled-channel calculations. This effect has been first pointed out by the present authors in Ref. 18.

According to Eq. (12a), the interaction leading to target excitation is

$$S^2\frac{Z_P}{r_P'}=\gamma Z_P(1-\beta\alpha_z)\left[\frac{1}{R'}+\frac{bx_T+\gamma^2vtz_T}{(R')^3}+\cdots\right], \tag{18}$$

where higher multipole terms have been omitted. In this

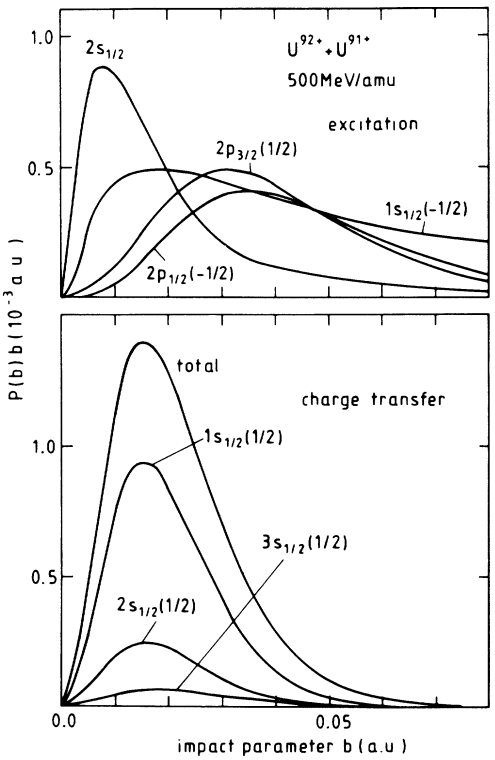

FIG. 3. Weighted excitation and capture probabilities $P(b)b$ for $U^{92+}+U^{91+}(1s_{1/2})$ collisions at 500 MeV/amu laboratory energy as a function of the impact parameter b. Only the leading probabilities into specific final states $nl_j(m_j)$ are plotted.

expression, the $1/R'$ term multiplied with the unit matrix has vanishing off-diagonal matrix elements. The Dirac α matrix and the second term in the large parentheses give rise to dipole selection rules. However, it should be noted that owing to

$$\alpha \equiv [(\alpha\cdot\nabla),\mathbf{r}]=\frac{i}{\hbar c}[H,\mathbf{r}]\ , \tag{19}$$

all matrix elements of α between degenerate states are zero. Therefore, we may distinguish the following three types of long-range interactions.

I. Matrix elements with $1/R'$ (i.e., monopole) separation dependence and dipole selection rules arising from the term $\beta\alpha_z/R'$ between nondegenerate states.

II. Matrix elements with $1/(R')^2$ (i.e., dipole) separation dependence and monopole or quadrupole selection rules arising from the term $\beta\alpha_z\gamma^2 z_T vt/(R')^3$.

III. Matrix elements with $1/(R')^2$ (i.e., dipole) separation dependence and dipole selection rules arising from the term $\gamma^2 vtz_T/(R')^3$ dominate if the type I matrix elements vanish.

Type-I as well as type-II interactions are of magnetic origin and do not survive if either the projectile or the electron motion tends to the nonrelativistic limit. In that case, type-III interactions prevail. All three types do not change the magnetic quantum numbers, and only higher-order terms in Eq. (18) with an $1/(R')^3$ dependence and monopole, dipole, or quadrupole selection rules are able to do that.

In Fig. 1 the curves for the excitation probabilities clearly demonstrate the existence and different separation dependences of the type-I and -II long-range interactions. In Fig. 2 the same is true, and only the transitions between the $2s_{1/2}$ and $2p_{1/2}$ states deserve particular attention. The latter appear to have a $1/R'$ separation dependence; however, because of the $2s_{1/2}$-$2p_{1/2}$ degeneracy and hence the absence of time oscillations in the transition amplitude, it is the indefinite time integral over a type-III interaction that is responsible for the behavior of the occupation curves. To be sure, we have in all cases confirmed our interpretation by a direct numerical calculation of the coupling matrix elements.

In contrast to excitation, the charge transfer probabilities exhibited in the lower part of Fig. 1 are all of short range since they depend on the overlap between target and projectile states. The corresponding diagrams for excited initial states (not shown here) have the same appearance.

In Fig. 3 we present weighted excitation and transfer probabilities $P(b)b$ for the leading transitions as a function of the impact parameters. As expected, the probabilities for excitation reach out to much larger impact parameters than for transfer. A particular role is played by the spin-flip transition $1s_{1/2}(\frac{1}{2})\rightarrow 1s_{1/2}(-\frac{1}{2})$. Being degenerate within our treatment, the two states are strongly coupled even at large impact parameters. In fact, the total cross section diverges logarithmically since the time integral over the matrix element of the transverse dipole part $\beta\alpha_z b x_T/(R')^3$ in Eq. (18) yields a dependence of $P(b)b$ as $1/b$. This divergence[25] is spurious and can be remedied by including higher-order QED corrections or hyperfine interactions removing the degeneracy. However, even with these corrections the estimated range in b space of the spin-flip transitions is much larger than for any other transitions, so that the latter remain unaffected by the former.

We already have remarked that the $U^{92+}+U^{91+}$ collision may serve as a testing ground for fully relativistic calculations. In Tables I and II we therefore present state-to-state cross sections for excitation and charge transfer obtained from a 36-state calculation. Within a single calculation using the same matrix elements, we have separately chosen the initial states as $1s_{1/2}(\frac{1}{2})$, $2s_{1/2}(\frac{1}{2})$, $2p_{1/2}(\frac{1}{2})$, $2p_{3/2}(\frac{1}{2})$, and $2p_{3/2}(\frac{3}{2})$ and subsequently have calculated the cross sections into all final states up to the $3p_{3/2}$ shell. In analogy to the spin-flip transition discussed above, the excitation cross sections between the degenerate states diverge. Inspection of Table I also reveals that detailed balancing $\sigma_{i\rightarrow f}=\sigma_{f\rightarrow i}$ holds within the calculated accuracy. Since these numbers have been derived from independent calculations, the agreement serves as a check on the numerical accuracy. A similar test for charge transfer comparing capture into the target with capture into the projectile has also been performed and has led to the same conclusion.

In Table III we compare the results of the present 36-state calculation with those of the previous 20-state ex-

TABLE I. Excitation cross sections (in barns) between target and projectile $nl_j(m_j)$ states in $U^{92+} + U^{91+}$ collisions at 500 MeV/amu laboratory energy. The 36-state close-coupling calculations include target and projectile K, L, and M shells. Diverging cross sections (see text) are indicated by div. The number in square brackets following the cross section gives the power of ten multiplying the preceding number.

Final \ Initial	$1s_{1/2}(\frac{1}{2})$	$2s_{1/2}(\frac{1}{2})$	$2p_{1/2}(\frac{1}{2})$	$2p_{3/2}(\frac{1}{2})$	$2p_{3/2}(\frac{3}{2})$
		Cross section (barns)			
$1s_{1/2}(\frac{1}{2})$		3.65[3]	1.96[3]	3.86[3]	3.19[3]
$1s_{1/2}(-\frac{1}{2})$	div	2.95[2]	3.49[3]	7.52[2]	6.35[1]
$n=1$ shell		3.95[3]	5.45[3]	4.61[3]	3.26[3]
$2s_{1/2}(\frac{1}{2})$	3.65[3]		div	8.59[4]	5.60[5]
$2s_{1/2}(-\frac{1}{2})$	2.95[2]	div	div	1.83[5]	1.23[3]
$2p_{1/2}(\frac{1}{2})$	1.96[3]	div		3.62[3]	1.60[4]
$2p_{1/2}(-\frac{1}{2})$	3.49[3]	div	div	1.05[4]	1.91[4]
$2p_{3/2}(\frac{3}{2})$	3.19[3]	5.60[5]	1.60[4]	div	
$2p_{3/2}(\frac{1}{2})$	3.86[3]	8.59[4]	3.62[3]		div
$2p_{3/2}(-\frac{1}{2})$	7.52[2]	1.83[5]	1.05[4]	div	8.11[3]
$2p_{3/2}(-\frac{3}{2})$	6.35[1]	1.23[3]	1.91[4]	8.11[3]	4.06[2]
$n=2$ shell	1.73[4]				
$3s_{1/2}(\frac{1}{2})$	7.09[2]	3.80[4]	9.91[2]	5.82[3]	1.48[4]
$3s_{1/2}(-\frac{1}{2})$	7.20[1]	1.05[3]	3.91[3]	5.26[3]	1.75[2]
$3p_{1/2}(\frac{1}{2})$	1.82[2]	2.00[4]	1.72[4]	2.44[3]	7.24[3]
$3p_{1/2}(-\frac{1}{2})$	2.25[2]	3.18[4]	3.60[3]	9.12[2]	7.76[3]
$3p_{3/2}(\frac{3}{2})$	2.94[2]	1.79[4]	4.35[2]	2.40[3]	3.07[4]
$3p_{3/2}(\frac{1}{2})$	3.83[2]	2.15[4]	9.10[2]	1.97[4]	1.11[4]
$3p_{3/2}(-\frac{1}{2})$	1.06[2]	6.30[3]	1.75[3]	7.40[3]	1.84[3]
$3p_{3/2}(-\frac{3}{2})$	5.87[0]	5.59[1]	1.53[3]	2.10[3]	3.60[1]
$n=3$ shell	1.98[3]	1.37[5]	3.03[4]	4.60[4]	7.37[4]

pansion.[18] The difference between the two sets of results is of the order of 10% or less. This suggests that the expansion has almost converged within the space of bound-basis states. While ionization channels have not been included explicitly, each atomic bound state on one center has an overlap with (positive- or negative-energy) continuum states on the other center within the interaction region reflecting a transient population of continuum states. The explicit inclusion of ionization channels in the basis expansion, similarly as in nonrelativistic calculations,[26] will not significantly change the rates for charge transfer. This can be inferred from the distinctly different range of ionization interactions on the one hand and capture on the other hand. Only at very small internuclear separations will both processes couple strongly,[16,17] but this region carries little weight for the total cross section. The insensitivity of charge transfer to the inclusion of ionization channels means that the unitarity requirement is satisfied at the expense of the initial state. In other words, the addition of further states leads to a depletion of the initial state rather than of competing final states. We also disregard the possibility of electron-positron pair production. The corresponding cross sections are negligible[27] and, more importantly, negative-energy compoments do not invalidate the unambiguous interpretation of the occupation amplitudes, since at $t \to \pm\infty$ our basis states are exact orthogonal eigenstates of the full Dirac Hamiltonian, having no overlap with the negative-energy continuum.

Having obtained rather detailed close-coupling results for the $U^{92}+U^{91+}$ test system, it is instructive to compare with the results of other theories. In Ref. 18 we have compared with the results of the Born approximation for excitation and with the results of the relativistic Born approximation satisfying Coulomb boundary conditions[15] (R1B) for charge transfer. For the energies of 1 and 0.5 GeV/amu, the perturbative results differ significantly in some cases from those of close-coupling (CC) calculations.[18] For charge transfer, we here present a more complete comparison in Table IV. In addition to R1B (Refs. 15 and 28) and OBK (Refs. 10 and 28) cross sections, we also include the prior and the post versions of relativistic eikonal approximation (EA) cross sections.[6-8,28] If one uses the nuclear charge as a criterion to choose between the prior and post forms, obviously none of them is preferred in a symmetric collision. However, if one chooses Z/n to gauge the strength of the interaction,[9,7] the excited projectile states effectively "see"

TABLE II. Electron transfer cross sections (in barns) between target and projectile $nl_j(m_j)$ states in $U^{92+} + U^{91+}$ collisions at 500 MeV/amu laboratory energy. See caption of Table I.

Final \ Initial	$1s_{1/2}(\frac{1}{2})$	$2s_{1/2}(\frac{1}{2})$	$2p_{1/2}(\frac{1}{2})$	$2p_{3/2}(\frac{1}{2})$	$2p_{3/2}(\frac{3}{2})$
	Cross section (barns)				
$1s_{1/2}(\frac{1}{2})$	3.98[3]	1.43[3]	2.25[2]	1.97[2]	4.51[1]
$1s_{1/2}(-\frac{1}{2})$	2.28[2]	7.47[1]	8.51[1]	5.73[1]	6.25[0]
$n=1$ shell	4.12[3]	1.51[3]	3.11[2]	2.54[2]	5.14[1]
$2s_{1/2}(\frac{1}{2})$	1.01[3]	4.55[2]	2.79[2]	2.44[2]	7.87[1]
$2s_{1/2}(-\frac{1}{2})$	4.84[1]	3.05[1]	1.73[2]	1.61[1]	5.43[0]
$2p_{1/2}(\frac{1}{2})$	3.06[2]	4.81[2]	2.22[2]	3.53[2]	4.82[1]
$2p_{1/2}(-\frac{1}{2})$	8.50[1]	2.32[2]	3.10[2]	4.34[1]	1.00[2]
$2p_{3/2}(\frac{3}{2})$	3.27[1]	9.86[1]	5.87[1]	1.15[2]	8.95[1]
$2p_{3/2}(\frac{1}{2})$	1.43[2]	4.46[2]	3.90[2]	4.13[2]	7.65[1]
$2p_{3/2}(-\frac{1}{2})$	5.08[1]	3.20[1]	2.11[1]	1.83[2]	4.16[1]
$2p_{3/2}(-\frac{3}{2})$	4.17[0]	5.35[0]	1.04[2]	3.66[1]	1.33[0]
$n=2$ shell	1.68[3]	1.78[3]	1.56[3]	1.40[3]	4.41[2]
$3s_{1/2}(\frac{1}{2})$	3.18[2]	1.66[2]	1.72[2]	2.15[2]	8.86[1]
$3s_{1/2}(-\frac{1}{2})$	1.46[1]	1.16[1]	1.35[2]	1.71[1]	3.34[0]
$3p_{1/2}(\frac{1}{2})$	8.32[1]	1.12[2]	9.13[1]	2.54[2]	4.21[1]
$3p_{1/2}(-\frac{1}{2})$	1.57[1]	5.52[1]	1.32[2]	3.14[0]	2.53[1]
$3p_{3/2}(\frac{3}{2})$	6.02[0]	2.52[1]	1.24[1]	3.11[1]	3.48[1]
$3p_{3/2}(\frac{1}{2})$	4.98[1]	1.25[2]	1.95[2]	2.51[2]	5.97[1]
$3p_{3/2}(-\frac{1}{2})$	1.46[1]	1.13[1]	2.86[1]	7.71[1]	1.24[1]
$3p_{3/2}(-\frac{3}{2})$	9.97[−1]	1.51[0]	2.62[1]	1.15[1]	2.28[−1]
$n=3$ shell	5.03[2]	5.06[2]	7.92[2]	8.60[2]	2.67[0]
sum $n \leq 3$	6.31[3]	3.79[3]	2.66[3]	2.52[3]	7.59[2]

a smaller charge, and hence one should use the prior form of the theory. We observe that the R1B cross sections in most cases have a magnitude intermediate between the prior- and post-form eikonal values. For some final subshells, the R1B results are close to the coupled-channel results; for others they deviate by as much as a factor of 2. The total K-shell capture cross sections are all in fair agreement with one another except for those of the OBK theory, which systematically yields cross sections that are one order of magnitude too high.[6–8] It might be remarked that the simple analytical formula of Ref. 6 for $1s_{1/2}$-$1s_{1/2}$ transitions (based on an αZ expansion) in conjunction with the scaling rule of Ref. 9 yields cross sections for higher shells that are considerably too large in this case.

B. Collision of Xe^{54+} with Ag and Au targets

Total cross sections have been measured[9,2] for a number of projectile-target combinations. We have chosen to compare our calculations with data for Xe^{54+} and Xe^{52+} ions incident on Ag and Au as representatives for a medium-heavy and heavy target atom. Measurements are available[9] for projectile energies of 82, 140, and 197 MeV/amu. As is already known from a previous analysis[9] based on the relativistic eikonal theory,[6] the K,

TABLE III. Excitation and capture cross sections (in barns) for 500 MeV/amu $U^{92+} + U^{91+}$ $(1s_{1/2})$ collisions calculated in 20-state (Ref. 18) and in 36-state expansions. The number in square brackets gives the power of ten by which the preceding number has to be multiplied.

Final shell	Cross section (barns) Excitation 20 states	Excitation 36 states	Capture 20 states	Capture 36 states
$1s_{1/2}$			4.18[3]	4.12[3]
$2s_{1/2}$	4.37[3]	3.94[3]	1.12[3]	1.06[3]
$2p_{1/2}$	5.19[3]	5.46[3]	4.20[2]	3.91[2]
$2p_{3/2}$	7.49[3]	7.81[3]	2.36[2]	2.30[2]

TABLE IV. Cross sections per electron (in barns) for K capture in collisions of $U^{92+} + U^{91+}$ at 500 MeV/amu. The columns show various theoretical results: CC, present 36-state coupled-channel calculations; R1B, relativistic boundary-corrected Born approximation (Refs. 15 and 28), EA prior and EA post are eikonal approximations (Refs. 6 and 28); OBK, relativistic OBK approximation (Refs. 10 and 28). The number in square brackets gives the power of ten multiplying the preceding number.

	Cross section (barns)				
Final shell	CC	R1B	EA prior	EA post	OBK
$1s_{1/2}$	4.12[3]	3.39[3]	4.14[3]	4.14[3]	4.91[4]
$2s_{1/2}$	1.06[3]	5.13[2]	7.62[2]	5.67[2]	5.28[3]
$2p_{1/2}$	3.91[2]	5.95[2]	1.35[3]	4.44[2]	9.02[3]
$2p_{3/2}$	2.31[2]	2.74[2]	1.24[3]	1.07[2]	7.61[3]
$3s_{1/2}$	3.28[2]	1.51[2]	2.30[2]	1.58[2]	1.41[3]
$3p_{1/2}$	1.03[2]	1.75[2]	4.37[2]	1.30[2]	2.60[3]
$3p_{3/2}$	7.25[1]	9.15[1]	4.62[2]	3.61[1]	2.56[3]
Sum	6.31[3]	5.19[3]	8.62[3]	5.58[3]	7.76[4]

L, and M shells of target and projectile all contribute to the total cross section, and to a lesser extent even higher shells. This reflects the fact that the energy range in which measurements have been made is adequate for nonperturbative coupled-channel calculations.

The theory presented in Sec. II is founded on a single-electron description. For multielectron targets, additional assumptions have to be made. Since transitions between occupied target shells cannot occur, we separately compute the contribution of each target substate to the capture cross section by including only this single target state in the two-center basis and "freezing" all other occupied target shells. On the projectile side, we couple all 28 states of the K, L, and M shells. Only for transitions from the target M shell do we restrict ourselves to the 18 lowest projectile states (up to the $3p_{3/2}$ subshell) in order to save computing time. All target subshells up to $2p_{3/2}$for Ag and up to $3p_{3/2}$ for Au are individually considered using effective charges $Z^* = Z_T$ for the K shell (a subtraction of 0.3 gives a negligible correction), $Z^* = Z_T - 4.15$ for the L shell, and $Z^* = Z_T - 11.0$ for the $3s$ and $3p$ shells.

Table V summarizes the cross sections from individual initial shells obtained in this way. The importance of higher target shells at these energies is clearly evident. Only at the higher projectile energies, there is some indication of convergence with increasing principal quantum number. Computing time puts a limitation to significantly extending the calculations to higher shells.

In Fig. 4 we present electron transfer cross sections from initial $1s_{1/2}$, $2s_{1/2}$, $2p_{1/2}$, and $2p_{3/2}$ shells into all subshells up to the $3d_{5/2}$ shell of the projectile at an energy of 197 MeV/amu. The cross sections given are averaged over initial and final substates. Both for Ag and Au targets, the $1s_{1/2} \rightarrow 1s_{1/2}$ cross section is the largest. However, for capture into higher projectile states, the be-

TABLE V. Cross sections (in barns) for charge transfer from Ag and Au subshells into the K, L, and M shells of Xe^{54+} at laboratory energies of 82, 140, and 197 MeV/amu. The number in square brackets gives the power of ten multiplying the preceding number.

Initial	Cross section (barns)		
shell	82 MeV/amu	140 MeV/amu	197 MeV/amu
Ag			
$1s_{1/2}$	9.46[4]	3.30[4]	1.42[4]
$2s_{1/2}$	2.39[4]	7.70[3]	3.19[3]
$2p_{1/2}$	2.85[4]	4.26[3]	1.14[3]
$2p_{3/2}$	2.59[4]	3.64[3]	9.24[2]
Sum	3.98[5]	1.04[5]	4.08[4]
Au			
$1s_{1/2}$	3.07[4]	1.97[4]	1.23[4]
$2s_{1/2}$	7.07[4]	1.52[4]	6.08[3]
$2p_{1/2}$	7.20[4]	2.22[4]	9.05[3]
$2p_{3/2}$	7.01[4]	1.92[4]	7.22[3]
$3s_{1/2}$[a]	1.55[4]	4.77[3]	2.34[3]
$3p_{1/2}$[a]	2.76[4]	7.99[3]	3.10[3]
$3p_{3/2}$[a]	2.75[4]	7.08[3]	2.48[3]
Sum	7.36[5]	2.45[5]	1.05[5]

[a]The sum over final M subshells does not include $3d_{3/2}$ and $3d_{5/2}$ states.

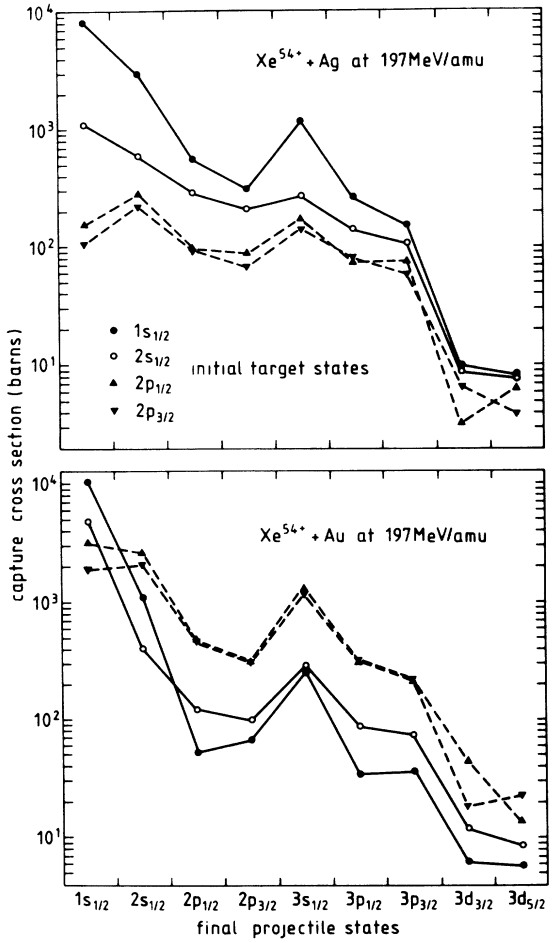

FIG. 4. State-to-state charge transfer cross sections for Xe^{54+} + Ag and Au collisions at 197 MeV/amu laboratory energy. The cross sections given are averaged over initial and final angular momentum projections within a subshell.

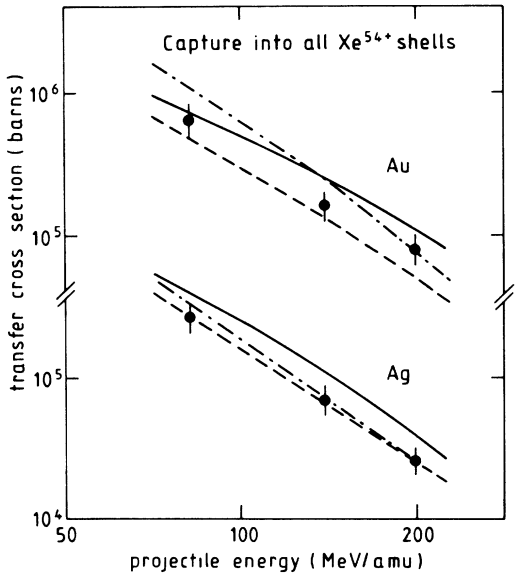

FIG. 5. Cross sections for charge transfer in collisions of Xe^{54+} with Au and Ag targets as a function of the laboratory projectile energy. The data points are from Refs. 9 and 20. The error bars include estimated 20% systematic errors. The solid lines represent the results of the present coupled-channel calculations. The dashed and dash-dotted lines are taken from Ref. 9 and show the results of two different eikonal (Ref. 6) calculations, see text.

havior of these targets is strikingly different. For Ag ($Z_T=47$) the projectile energy significantly exceeds the K-shell matching energy $E_m=55$ MeV/amu, so that the initial and final $1s_{1/2}$ and $2s_{1/2}$ shells with their large momentum components contribute most to the cross sections. Conversely, for Au ($Z_T=79$) the projectile energy is close to $E_m=170$ MeV/amu, so that energy matching of the wave functions plays a more important role.

In Fig. 5, experimental[20] and theoretical total cross sections for Xe^{54+} + Ag and Xe^{54+} + Au have been summarized. The eikonal cross sections[6] indicated by dashed and dash-dotted lines have been taken from Ref. 9. They differ by the criterion used to choose between the post and prior versions of the theory. For the dash-dotted and for the dashed curve the values of Z/n and Z, respectively, have been adopted to determine the stronger interaction and hence the choice between post and prior.[9,7] The solid line represents the results of the present coupled-channel calculations. While for Au they are in reasonable agreement with the data, they overestimate the cross section for Ag by 20–40 %.

An independent piece of experimental information can be extracted from existing capture data for Xe^{52+} projectiles at the same energies.[9,20] Aside from a small screening correction, we may approximately identify[20]

$$\sigma_{\text{tot}}(Xe^{54+})-\sigma_{\text{tot}}(Xe^{52+})=\sigma_K(Xe^{54+}) , \tag{20}$$

where $\sigma_K(Xe^{54+})$ is the cross section for capture into the

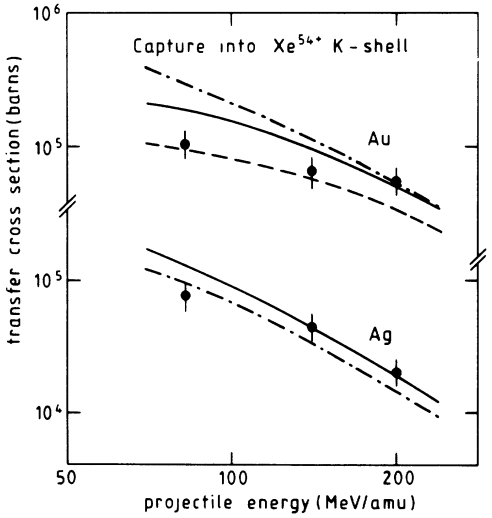

FIG. 6. Cross sections for charge transfer into the projectile K shell in Xe^{54+} + Au and Xe^{54+} + Ag collisions as a function of the laboratory projectile energy. The data points have been obtained according to Eq. (20) of the text. The notation for the theoretical curves is the same as in Fig. 5. For Ag targets the two eikonal versions coincide.

K shell of Xe^{54+}. To the extent that Eq. (20) is valid, we can directly compare this number with the corresponding theoretical value and thus eliminate the contribution from excited and continuum states of the projectile. This has been done in Fig. 6. The experimental points have been obtained from Eq. (20) and the solid line from Table V. The exact eikonal curves are calculated from Ref. 6 using the same two versions as in Fig. 5. For Ag targets both versions coincide. We observe that the agreement with these more specific experimental data is quite satisfactory, in particular for the higher energies. The data point for Au at 140 MeV seems to be too low in Figs. 5 and 6, as judged from the systematics. For the lowest energy (where anyhow convergence is incomplete), another effect besides screening corrections may play a role in limiting the applicability of Eq. (20): For Xe^{52+} the K shell is forbidden not only as a final state but also as an intermediate state during the collision. This is in contrast to theoretical Xe^{54+} calculations in which all intermediate states are accessible. Clearly, multistep processes will be more important at lower energy so that a larger discrepancy may be expected there.

This example illustrates that it would be highly desirable to have experimental data for specific transitions in which at least the initial or the final state is detected. A comparison with a detailed theory like the present one then would be much more meaningful.

V. SUMMARY AND CONCLUSIONS

We have presented here for the first time a detailed account of fully relativistic coupled-channel calculations[18] for atomic collisions between high-Z projectiles and high-Z targets. Using a two-center atomic expansion in terms of exact hydrogenic Dirac eigenstates we have been able to give detailed predictions for single-electron excitation and charge transfer cross sections between specific atomic states.

It has been demonstrated that relativistically induced magnetic effects give rise to unusual long-range couplings[18] which affect certain partial cross sections. These couplings have been classified with regard to their selection rules and their dependence on the internuclear separation. Several examples have been presented and discussed.

The coupled-channel method has been systematically applied to collisions of $U^{92+}+U^{91+}$ and $Xe^{54+}+Ag$ and $Xe^{54+}+Au$. In all cases we have included initial and final excited states. In fact, at these high atomic numbers, charge transfer from excited target states and to excited projectile states plays an important role.

The collision of $U^{92+}+U^{91+}$ at 500 MeV/amu serves as a testing ground for relativistic theories. We have studied the time evolution of the occupation probabilities, the impact parameter dependence of the cross sections, and the convergence properties by increasing the size of the basis set from 20 states[18] to 36 states. We found that the addition of 18 M-shell basis states changed the cross sections within the K and L shells by 10% or less. We have also compared with the results of other calculations. While the R1B approximation[15] and the eikonal theory[6] give total cross sections roughly similar to the coupled-channel method, they deviate considerably in certain partial cross sections.

For collisions of $Xe^{54+}+Ag$ and $Xe^{54+}+Au$ at 82, 140, and 197 MeV/amu we have been able to compare the results of our calculations with existing experimental data for charge transfer.[9,20] We found good agreement with the data for Au targets but our results slightly overestimate the total cross sections for Ag targets. As an independent piece of information, we have extracted approximate cross sections for charge transfer into the K shell of Xe^{54+} projectiles from Xe^{54+} and Xe^{52+} total capture data.[9,20] These cross sections were well represented by our calculations except for the lowest energy, where incomplete convergence and blocking effects play a role.

In summary, we have shown that accurate calculations for excitation and charge transfer in collision systems of particular experimental interest are becoming possible. The main limitation is given by the availability of computer time.

ACKNOWLEDGMENTS

The authors wish to thank Professor W. E. Meyerhof for communicating unpublished results and for proposing to extract experimental projectile K-capture data from Xe^{54+} and Xe^{52+} total cross sections. We also acknowledge helpful discussions with Dr. W. Fritsch.

---

*Permanent address: Institute of Applied Physics, University of Tsukuba, Tsukuba, Ibaraki 305, Japan.

†Also at Fachbereich Physik, Freie Universität Berlin, D-1000 Berlin 39, Federal Republic of Germany.

[1]C. T. Munger and H. Gould, Phys. Rev. Lett. **57**, 2927 (1986); H. Gould and C. T. Munger, in *Atomic Physics 10,* edited by H. Narumi and I. Shimamura (North-Holland, Amsterdam, 1987), p. 95.

[2]For a review of earlier experimental and theoretical work, see R. Anholt and H. Gould, Adv. At. Mol. Phys. **22**, 315 (1986).

[3]For a review of electromagnetic processes, see C. A. Bertulani and G. Baur, Phys. Rep. **163**, 299 (1988).

[4]R. Anholt, W. E. Meyerhof, Ch. Stoller, E. Morenzoni, S. A. Andriamonje, I. D. Molitoris, O. K. Baker, D. H. H. Hoffmann, H. Bowman, J. S. Xu, Z. Z. Xu, K. Frankel, D. Murphy, K. Crowe, and J. O. Rasmussen, Phys. Rev. A **30**, 2234 (1984).

[5]U. Becker, N. Grün, and W. Scheid, J. Phys. B **18**, 4589 (1985).

[6]J. Eichler, Phys. Rev. A **32**, 112 (1985).

[7]J. Eichler, in *Electronic and Atomic Collisions,* edited by D. C. Lorents, W. E. Meyerhof, and J. P. Peterson (North-Holland, Amsterdam, 1986), p. 257; Nucl. Instrum. Methods Phys. Res. Sec. B **23**, 23 (1987).

[8]R. Anholt and J. Eichler, Phys. Rev. A **31**, 3505 (1985).

[9]W. E. Meyerhof, R. Anholt, J. Eichler, H. Gould, Ch. Munger, J. Alonso, P. Thieberger, and H. E. Wegner, Phys. Rev. A **32**,

3291 (1985).
[10]B. L. Moisewitsch and S. G. Stockman, J. Phys. B **13**, 2975 (1980); R. Shakeshaft, Phys. Rev. A **20**, 729 (1979).
[11]W. J. Humphries and B. L. Moisewitsch, J. Phys. B **17**, 2655 (1984); B. L. Moiseiwitsch, Phys. Rep. **118**, 133 (1985).
[12]D. H. Jakubassa-Amundsen and P. A. Amundsen, Z. Phys. A **298**, 13 (1980).
[13]G. R. Deco and R. D. Rivarola, J. Phys. B **19**, 1759 (1986); G. R. Deco, Ph.D. thesis, University of Rosario, Argentina, 1987.
[14]B. L. Moisewitsch, J. Phys. B **19**, 3733 (1986); **20**, L171 (1987); G. R. Deco and R. D. Rivarola, *ibid.* **20**, 317 (1987).
[15]J. Eichler, Phys Rev. A **35**, 3248 (1987); **37**, 287(E) (1988). The results quoted here have been computed with the exact version. For the nonrelativitsic case, see also D. P Dewangan and J. Eichler, Comments At. Mol. Phys. **21**, 1 (1987).
[16]U. Becker, N. Grün, W. Scheid, and G. Soff, Phys. Rev. Lett. **56**, 2016 (1986).
[17]U. Becker, Ph.D. thesis, University of Giessen, West Germany, 1986.
[18]N. Toshima and J. Eichler, Phys. Rev. Lett. **60**, 573 (1988).
[19]W. Fritsch and C. D. Lin, in *Electronic and Atomic Collisions,* edited by J. Eichler, I. V. Hertel, and N. Stolterfoht (North-Holland, Amsterdam, 1984), p. 33.
[20]W. E. Meyerhof (private communication). A detailed analysis has slightly modified some of the values of Ref. 9.
[21]J. J. Sakurai, *Advanced Quantum Mechanics* (Addison-Wesley, Reading, MA, 1967).
[22]J. D. Jackson, *Classical Electrodynamics,* 2nd ed. (Wiley, New York, 1975), Sec. 11.
[23]N. Toshima, T. Ishihara, and J. Eichler, Phys. Rev. A **36**, 2659 (1987).
[24]M. E. Rose, *Relativistic Electron Theory* (Wiley, New York, 1961); J. D. Bjorken and S. D. Drell, *Relativistic Quantum Mechanics* (McGraw-Hill, New York, 1964).
[25]N. Toshima, J. Phys Soc. Jpn. **42**, 633 (1977).
[26]T. G. Winter, Phys. Rev. A **25**, 697 (1982); W. Fritsch and C. D. Lin, *ibid.* **27**, 3361 (1983).
[27]U. Becker, N. Grün, and W. Scheid, J. Phys. B **20**, 2075 (1987).
[28]The cross sections quoted here have been obtained by a direct numerical integration of the exact R1B, EA, and OBK expressions.